Numerical Methods in Civil Engineering, 6-3 (2022) 64-77

**Numerical Methods in Civil Engineering**

Journal Homepage: https://nmce.kntu.ac.ir/

# Effect of the angle of seismic incidence on the response of a long-span curved bridge under spatially varying ground motions

**Aziz Hosseinnezhad* and Amin Gholizad****

*ARTICLE INFO*

RESEARCH PAPER

*Article history:*
*Received:*
*June 2021.*
*Revised:*
*October 2021.*
*Accepted:*
*December 2021.*

*Keywords:*
*SVGMs;*
*seismic incidence angle;*
*wave passage;*
*lagged coherency;*
*site response*

***Abstract:***

*The incidence angle of seismic waves affects the maximum response of bridges. Furthermore, long-span structures experience different seismic excitations at supports because of the spatial variability of ground motions. Moreover, for curved bridges, because of the irregular shape and the interaction between bending and torsion, the maximum response of the structure would be correlated to the input angle of the earthquake. In this study, the dynamic response of a long-span reinforced concrete curved bridge under asynchronous input motions for different inclinations of seismic incidence was investigated. For the numerical study, a curved plan bridge from the Caltrans bridges portfolio is selected and analyzed for various load and soil scenarios. The correlated arrays are generated by the method described in the paper and implemented to investigate the bridge. From the outcomes, the directionality effect of ground motions is evident that the responses change corresponding to the input angle of the seismic wave. For the case of multiple support excitations, the maximum response is different from the uniform load pattern. Finally, to find the most unfavorable input angles, an incremental dynamic analysis was performed. The results showed that the maximum response for each column occurs for different angles of earthquake incidence. The results showed that the responses of the structure increased under some angles of incidence. Additionally, responses from multiple-support were more varied in comparison with uniform excitations under different input angles, and in some cases larger than the responses caused by uniform excitations.*

## 1. Introduction

A large number of devastating earthquakes have occurred since the 1970s and have destroyed a large number of bridges in the world. But it was after the San Fernando earthquake that many researchers severely focused on the seismic response of long-span bridges under the earthquake excitations. The length of the structure caused the seismic responses to be different from the same result obtained from ordinary bridges. One of the most important parameters which affect the seismic response of the mentioned structures is the input angle of the designated earthquake. There are few papers that take into account the issue of the influence of the input angle of the seismic wave on the maximum response of bridges.

** Ph.D. Student of Structural Engineering, Department of Civil Engineering, University of Mohaghegh Ardabili, Ardabil, Iran.*

***Corresponding author: Professor, Department of Civil Engineering, University of Mohaghegh Ardabili, Daneshgah Street, Ardabil, Iran. Email: Gholizad@uma.ac.ir*

Researchers over the past decades have studied the seismic behavior of long-span bridges under the excitations of ground movements. The main subject of the experimentations was to investigate the response of the studied bridge structures to seismic waves based on the type of structure and their orientation to the input seismic wave. Based on the mentioned papers and technical reports it is clear that none of these researchers considered the effects of spatial variations of seismic waves [1,2,3,4,5,6,7,8,9]. It is evident that all of them used deterministic approaches with the assumption of uniform excitation, and the issue of non-uniform excitation was almost neglected.

Recently, Wang et al. (2017) evaluated the directionality effect of ground motion on the responses of skewed bridges retrofitted with buckling restrained braces. They examined the structure for different angles of incidence, and the results showed that the seismic behavior of skewed bridges could be significantly different from that of straight bridges [10]. Roy et al. (2017) introduced a new damage index for evaluating the vulnerability of the studied bridges. They excited the structures under bi-directional seismic waves



[ DOR: 20.1001.1.23454296.2022.6.3.3.8 ]

[ DOI: 10.52547/nmce.6.3.64 ]

and, the corresponding results verified with the 30% rule. However, they neglected the spatial variations of the ground motions [11]. Soleimani et al. (2017) studied the responses of three various RC bridges to the seismic waves. They defined some uncertainties like skewness, unbalanced stiffness, and the height of columns to evaluate the seismic demand of the analyzed structures. The outcomes revealed that the parameters such as the intensity of seismic waves, columns radius, span length, and the compressive strength of concrete strongly affect the responses of the bridges. Nevertheless, the issue of non-uniform excitations was neglected [12]. Noori et al. (2017) investigated the effect of seismic input angles on the response of a curved bridge, including soil-structure interactions. They found that the maximum response of the bridge occurs for input angles between 30 to 50 degrees. Also, the results revealed that the SSI effects induce the responses. Even so, the effects of spatially varying ground motions were not considered [13]. In another study accomplished by Soltanieh et al. (2019), the effects of directionality of seismic waves on the responses of irregular bridges were explored. They modeled a five-span highway bridge, and the effect of soil-structure interactions were also considered. The results showed that the irrigularity, seismic incident, and the foundation condition are independent parameters that affected the fragility of the bridges. Meanwhile, the study did not considere the effect of the non-uniform excitations [14]. Wang et al. (2020) investigated the effects of directionality of seismic waves on the fragility of a skewed reinforced concrete bridge. They found that the responses of the bridge are not sensitive to the directionality of the input wave, and the maximum responses can be evaluated by the responses in longitudianl and transverse directions [15]. Feng et al. (2020) developed a method to evaluate the maximum response of a curved bridge for the different seismic incidents. To verify the results, an experimental sample bridge was utilized, and the outcomes indicated that the method has acceptable accuracy in evaluating the input seismic angles [16]. Ramos-Sepulveda and Cabas, (2021) investigated the effect of site condition on the directionality of ground motions and the corresponding effects on the seismic response of structures. They found that the site condition affects the directionality of input seismic waves [17]. Although recent studies have addressed the effect of seismic wave orientation, none of them have addressed the seismic wave spatial variability. In this research, the directionality of spatially variable seismic ground motions on the seismic response of a long-span bridge is investigated. Based on previous studies, it is found that the traveling ground motions are a function of time and space. Normally to analyze a structure under seismic waves, it is common that the variations in time are considered but spatial variations are ignored. Therefore, in this method, it is assumed that the structure is oscillating simultaneously and under the same acceleration at the whole length. In practice, however, this view is not correct for large-scale structures such as long-span bridges, as such structures experience different accelerations along the supports. It is also generally recognized that in multiple-support systems, such as bridges and dams, each support might be excited differently than the others due to the distance between supports and the differences in geologic and topographic features at their locations. For a seismic wave, the variation in velocity, refraction, and reflection, and soil profile changes cause asynchronous excitations for long structures such as bridges. Three components are generally defined to express the spatial variations of ground motion: (i) the velocity difference between traveling ground motions that is defined as wave passage, (ii) the variation in the frequency content caused due to refraction and reflection of ground motion during the crossing of soil beneath supports, which is defined as an incoherence parameter, (iii) and the variation of soil profile which is introduced as local site conditions. The results of some research have shown that the effect of spatial variation of ground motions on structures can be very destructive [18]. Based on the technical papers, two methods are developed for simulating the correlated ground motions, in which, both the defined power spectral density function and a coherency model are necessary to generate simulated time series. If the generated ground motions conditioned to a real array, the method is named conditional simulation method [19,20,21,22]. In this study, a method introduced and developed by Der Keuringihan and Konakli (2011) that considers all three spatially varying ground motions (SVGMs) parameters are used to generate correlated ground motions [22]. Then to explore the effect of the angle of seismic incidence of SVGMs, a prototype Caltrans curved plan bridge is selected and modeled in the OpenSEES platform. The simulated records were used to analyze the bridge in different input angles, and the results were compared and discussed.

## 2. Simulation of Correlated Ground Motions

Series of zero-mean and jointly stationary Gaussian acceleration processes are assumed at *n* sites on the ground described by auto-PSDs $G_{kk}(\omega)$, *k=1, 2,…, n,* and cross-PSDs $G_{kl}(\omega)$, *k, l=1, 2,…, n,* $k \neq l$. For each process, N is the number of discrete observations sampled at equal time intervals $\Delta t$. We denote the corresponding time instants as $t_i = i\Delta t$, *i=0… N−1*. The Fourier representation of such series is defined in [20]:

$$a_k(t_i) = A_{0k} + \sum_{p=1}^{\frac{N}{2}-1} \left[A_{pk} * cos(\omega_p t_i) + B_{pk} * sin(\omega_p t_i)\right] + (-1)^i * A_{(\frac{N}{2})k} \quad k = 1,2,\dots,n \qquad (1)$$


[ DOR: 20.1001.1.23454296.2022.6.3.3.8 ]
[ DOI: 10.52547/nmce.6.3.64 ]

Where N, introduces the number of separated observations specimens at equal time intervals $\Delta t$, $\omega_p = \frac{2\pi p}{N\Delta t}$ and $\{A_{pk}, B_{pk}\}$ are the Fourier coefficients. The Fourier coefficients are zero-mean, jointly Gaussian random variables that are uncorrelated for different frequencies, that is, $E[A_{pk}A_{qk}] = E[B_{pk}B_{qk}] = E[A_{pk}B_{qk}] = 0$ for $p \neq q$. At frequency $\omega_p$, the following relations hold,

$$E[A_{pk}A_{pl}] = E[B_{pk}B_{pl}] = \begin{cases} G_{kk}(\omega_p)\Delta\omega, & if\ k = l \\ Re[G_{kl}(\omega_p)]\Delta\omega, & if\ k \neq l \end{cases}$$
$$E[A_{pk}B_{pl}] = -E[B_{pk}A_{pl}] = \begin{cases} 0 & if\ k = l \\ -Im[G_{kl}(\omega_p)]\Delta\omega, & if\ k \neq l \end{cases} \quad (2)$$

Thus, for a defined auto-PSDs and cross-PSDs, it is possible to give all the variances/covariances of Fourier coefficients. The cross-PSD between the arrays at sites k and l is defined by the corresponding auto-PSDs through the relation:

$$G_{kl}(\omega) = \gamma_{kl}(\omega) * |G_{kk}G_{ll}(\omega)|^{0.5} \quad (3)$$

In which $\gamma_{kl}(\omega)$ is the coherency function and characterizes the SVGMs in the frequency domain.

Considering SVGMs studies, there are three significant phenomena that cause the spatial variation of ground motion [18]: the wave passage effects, the incoherence effects, and the local site effects. Two approaches were introduced to simulate the correlated earthquake ground motions, unconditioned and conditioned models. In both methods, a coherency model that describes the spatial variability of ground motion random field in the frequency domain, a seed of accelerogram at a specific location, and the Frequency Response Function of soil column beneath the foundations is necessary. In this study, the conditional simulation method and the Northridge earthquake acceleration time history are used to generate the correlated ground motions at all supports. The coherency for two supports at stations k and l are represented as below [20]:

$$\gamma_{kl}(\omega) = |\gamma_{kl}(\omega)| * exp\{i * [\theta_{kl}^{wp}(\omega) + \theta_{kl}^{sr}(\omega)]\} \quad (4)$$

In which $|\gamma_{kl}(\omega)|$ is the incoherence effect, $\theta_{kl}^{wp}(\omega)$ is introduced as wave passage and the site effects are defined as, $\theta_{kl}^{sr}(\omega)$.

Luco and Wang (1986), introduced an incoherence function that is used by many researchers [23]:

$$|\gamma(\varepsilon, \omega)| = exp\left[-\left(\frac{\alpha d_{kl}\omega}{v_s}\right)^2\right] \quad (5)$$

where $d_{kl}$ is the interval among stations $k$ and $l$, $v_s$ describes the average shear wave velocity, and $\alpha$ is the incoherence which can be found from data presented in [24] and [25]. The phase angle due to wave passage has been introduced as [23]:

$$\theta_{kl}^{wp}(\omega) = -\frac{\omega d_{kl}^L}{v_{app}} \quad (6)$$

In which $v_{app}$ is defined as surface apparent wave velocity and, $d_{kl}^L$, is the horizontal interval between stations $k$ and $l$. In the current study, the bridge is situated on the 6 supports. The distances between each support defines the corresponding $d_{kl}^L$. In other words, for the bridge, 38.6, 45.7,45.7, 45.7 and 38.6 are the horizontal intervals between stations. The phase angle due to the site-response effect is defined as [25]:

$$\theta_{kl}^{sr} = tan^{-1}\frac{Im|H_k(\omega)H_l(-\omega)|}{Re|H_k(\omega)H_l(-\omega)|} \quad (7)$$

In which $H_k(\omega)$ is the frequency response function (FRF).

Therefore, despite the non-stationary specifications of seismic ground motions, it is necessary to consider them stationary for simulation. So, the array is divided into some segments that are nearly stationary. Then, the simulation process is performed for each component, and the final array is made by assembling the simulated parts. Two methods are defined by Vanmarke and Fenton for simulation of a seismic wave [19]. The first method uses a general PSD (like white noise) to generate the random processes, named as the unconditional method, and the second one implements a known realization (a defined seismic record) to produce the random arrays called conditional simulation method. To better understand the simulation process of seismic ground motions, reference number 22 is recommended.

## 3. Numerical Study

For numerical study, a reinforced concrete bridge from the Caltrans bridge portfolio was selected and modeled by the OpenSEES platform. The bridge's characteristics were taken from a PEER Center prototype bridge portfolio that introduced different deck and bent solutions defined for California [26]. The schematic of the selected bridge is illustrated in Figure 2. The bridge is curved in plan and has a radius of 304.8 meters. The features of the deck shown in Table1, and Table 2 present the mechanical properties of the concrete and steel materials. Tables 3 and 4 represent the characteristics of columns and abutments. The elastic beam element is used to model the bridge deck and is assumed to remain uncracked. This assumption is correct due to the high stiffness of the deck elements. The deck is divided into 150 segments to provide a better approximation. The force-based fiber-section beam-column element was implemented to simulate the behavior of the columns [27]. The connection between columns and the deck is made by rigid links. To model the abutments, non-linear zero Length elements were used (Table 4) and the shear wave velocity was obtained from PEER (Table 5). The accuracy of the bridge finite element model was verified by the results of Tondini and


[ DOR: 20.1001.1.23454296.2022.6.3.3.8 ]
[ DOI: 10.52547/nmce.6.3.64 ]

Stojadinovic [28] and Amjadian and Agrawal [29]. The results of the current study by the mentioned papers are compared and shown in Table 6.

**Table 1**. The properties of the deck

| | | |
|---|---|---|
| Area | A | 6.0 $\mathbf{m^2}$ |
| Compressive Strength | $f'_{c.deck}$ | 35.0 N/mm^2 |
| Elasticity Modulus | E | 27597 N/mm^2 |
| Shear Modulus | G | 11500 N/mm^2 |
| Moment of Inertia About y-Axis | $I_z$ | 2.80 $m^4$ |
| Moment of Inertia About z-Axis | $I_y$ | 54.0 $m^4$ |
| Torsional Moment | $J_t$ | 6.0 $m^4$ |
| Prestress Force | $F_P$ | 31140 KN |

**Table 2**. The characteristics of the used materials

| | | |
|---|---|---|
| Confined Concrete | | |
| Compressive strength | $f'_{cc}$ | 47.0 N/mm^2 |
| Strain at $\mathbf{f'_{cc}}$ | $\varepsilon_{cc}$ | 0.0089 |
| Crushing strength | $f_{cu}$ | 39.0 N/mm^2 |
| Crushing strain | $\varepsilon_{cu}$ | 0.0365 |
| Elasticity modulus | $E_c$ | 24692 N/mm^2 |
| Tensile strength | $f_t$ | 2.8 N/mm^2 |
| Unconfined Concrete | | |
| Compressive strength | $f'_{co}$ | 28.0 N/mm^2 |
| Strain at $\mathbf{f'_{co}}$ | $\varepsilon_{psco}$ | 0.002 |
| Crushing strength | $f_{pcu}$ | 0.0 N/mm^2 |
| Sapling strain | $\varepsilon_{sp}$ | 0.005 |
| Steel | | |
| Yield Force | $f_{ye}$ | 471 N/mm^2 |
| Elasticity | $E_s$ | 200000 N/mm^2 |

In the vertical and transverse, the stiffness of the soil is computed and assigned to elastic zero Length elastic elements. The column's bottom ends are fixed. The average shear wave velocity was obtained from the PEER report, which is illustrated in Table 5 [32].

In this study, it is assumed that the wave propagates at various angles. So the finite element model of the structure is defined as rotate by a pre-defined angle (Figure 2).

To explore the critical angle, the bridge was subjected to 20 series of simulated arrays, and for each series, the angle varied from 0.0 to 90 degrees. The apparent wave velocity is defined based on a method developed by Kenzo and Yanabu.

To consider the local site effects, in the current study, based on the information in Table 5, it is assumed that the soil condition at simulation points 1 and 6 is type C, at simulation points 2, and 5, is type D, at simulation points 3, and 4 is type E. To generate the correlated ground motions, the Northridge earthquake record is selected and the required time series developed by using the conditional simulation method. Considering Figure 2, there are six simulation points, in which the first one is situated at the first abutment and the other points at the locations of columns 1, 2, 3, 4, and end abutment.

The incoherence parameter was introduced by many researchers. In this study, the amounts of 0.2 and 0.4 were considered weak, and strong incoherence, respectively [22].

The materials Concrete01, Concrete02 and Steel02, were used for unconfined, confined concrete and rebar, respectively. The specifications of used materials are illustrated in Tables 2 and 3.

In Table 4, the back wall and wing wall are reinforced concrete walls connected to the abutments. The back walls are situated in the direction perpendicular to the longitudinal axis of the bridge, and the wing walls are situated parallel to the longitudinal axis of the bridge.

**Table 3.** Mechanical properties of columns

| | |
|---|---|
| Yield curvature $\boldsymbol{\varphi_y}$ ($\frac{\mathbf{rad}}{\mathbf{m}}$) | 0.0039 76 |
| Yield moment $\mathbf{M_y}$ **(kNm)** | 6650 |
| Plastic moment $\mathbf{M_p}$ **(kNm)** | 8985 |
| Nominal shear strength $\mathbf{V_n}$ **(kN)** | 6278 |
| $\mathbf{M_p/V_n\,d}$ | 1.17 |
| Shear span to depth ratio longitudinal $\mathbf{H_{col}/2d}$ | 2.75 |

**Table 4**. Characteristics of Abutments [30-31]

| | |
|---|---|
| Back wall with | 8.0 m |
| Wing wall with | 4.0 m |
| $\mathbf{K_{abt}}$ **long** | 101811 kN/m |
| $\mathbf{P_{bw}}$ **long** | 3860 kN |
| $\mathbf{K_{abt}}$ **trans** | 243753 kN/m |
| $\mathbf{P_{bw}}$ **trans** | 1656 kN |
| $\boldsymbol{\rho}$ | 1760 $kg/m^3$ |
| $\mathbf{v_s}$ | 150 $m/s$ |
| $\mathbf{E_{soil}}$ | 110972 MPa |

**Table 5**: Average Shear wave velocity [32]

| Site Class | Soil Profile Name | $\mathbf{V_{s30}}$ |
|---|---|---|
| A | Hard Rock | >1500 m/s |
| B | Rock | 760 to 1500 m/s |
| C | Very Dense Soil and Soft Rock | 360 to 760 m/s |
| D | Stiff Soil | 180 to 360 m/s |
| E | Soft Soil | <180 m/s |

### *3.1 Simulated Ground Motions*

Based on a paper by Konakli and Der Keurighian, a Matlab code was developed and correlated arrays considering wave-passage, incoherence, and local site effects were generated [22]. Figures 3(a) and 3(b) illustrate the acceleration response spectrum and simulated time series, respectively. From Figure 3(a), at the first simulation point, the acceleration response spectrum of simulated arrays wholly fitted the original record.


[ DOR: 20.1001.1.23454296.2022.6.3.3.8 ]
[ DOI: 10.52547/nmce.6.3.64 ]

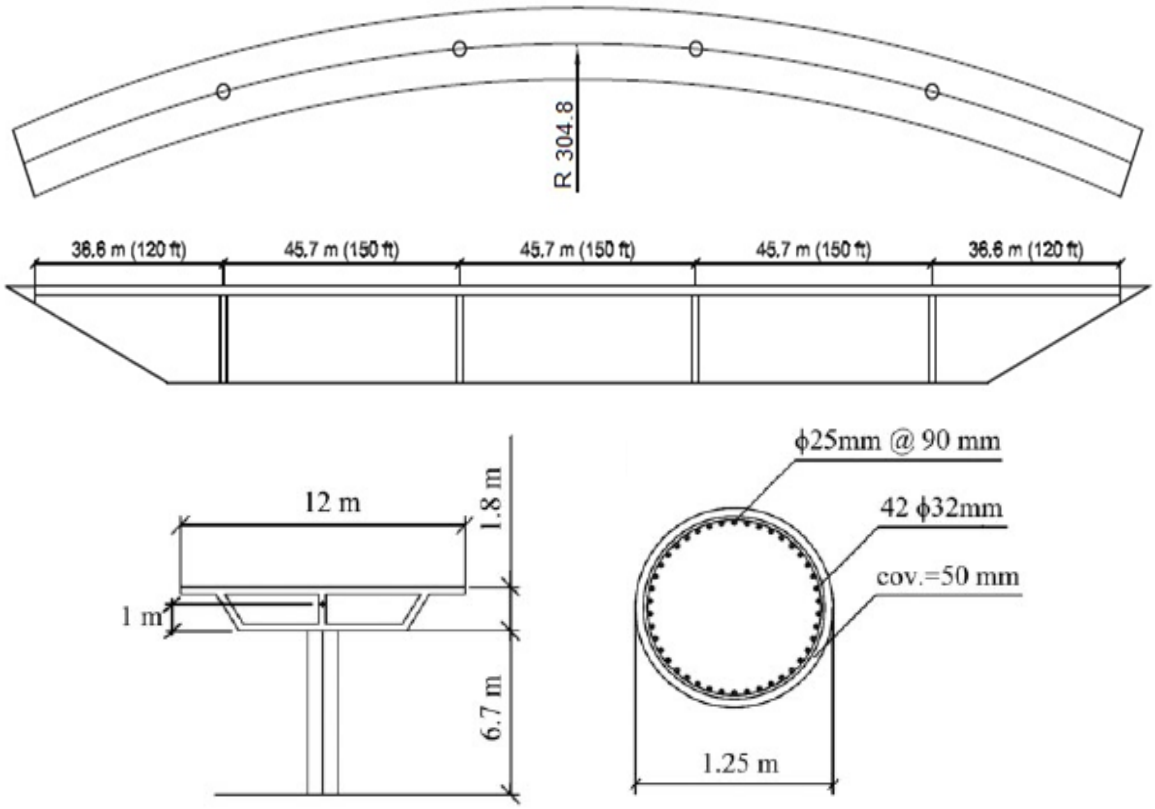


**Fig. 1.** Plan and view (a), deck section (b) and column section (c) of the bridge [29]

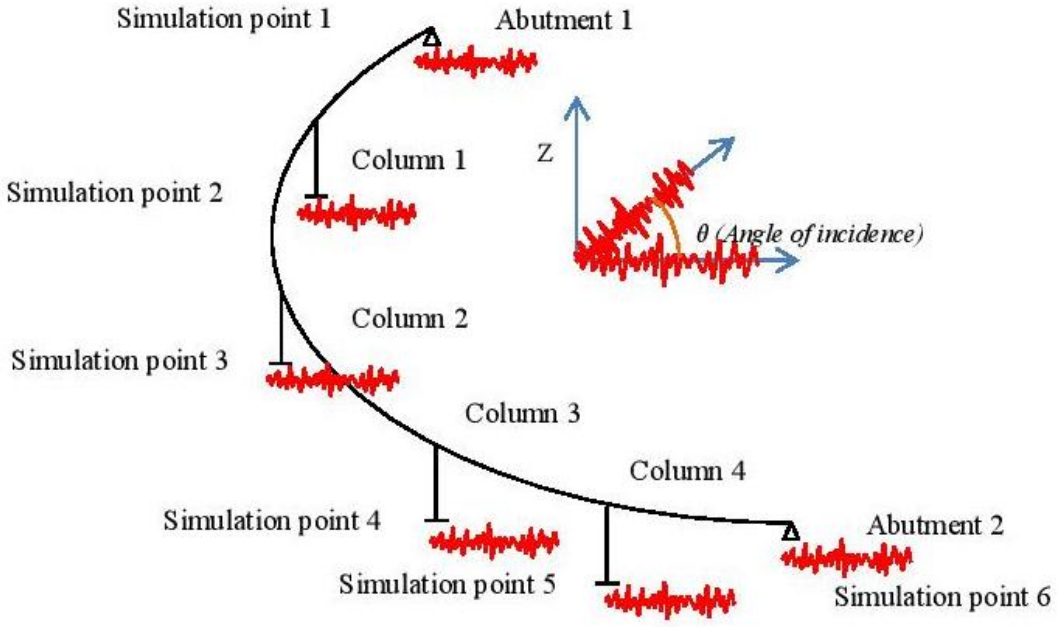


**Fig. 2.** Schematic representation of the bridge

However, the soil conditions for simulation points 1 and 6 are assumed to be the same, and the effects of SVGMs have led to two different records. The simulation process of spatially correlated ground motions has been completely presented by Konakli and Der Keurighian [20]. It is recommended that readers refer to the paper for a detailed study.

### *3.2 Dynamic characteristics of the bridge*

Table 6 shows the natural periods and frequencies of the bridge for the first 4 modes. The first transverse mode is the predominant mode of the bridge Tondini-Stojadinovic, and Amjadian-Agrawal. Figures 4, (a), (b), and (c) illustrate the first three mode shapes.


[ DOR: 20.1001.1.23454296.2022.6.3.3.8 ]
[ DOI: 10.52547/nmce.6.3.64 ]

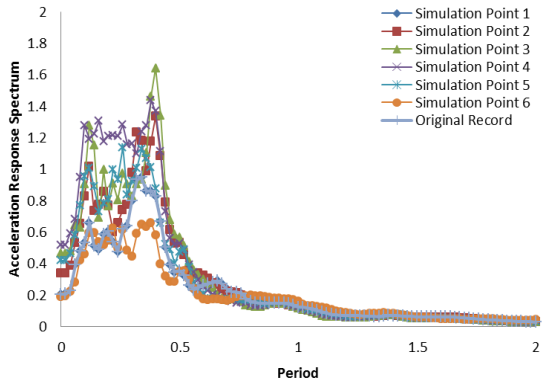


(a)

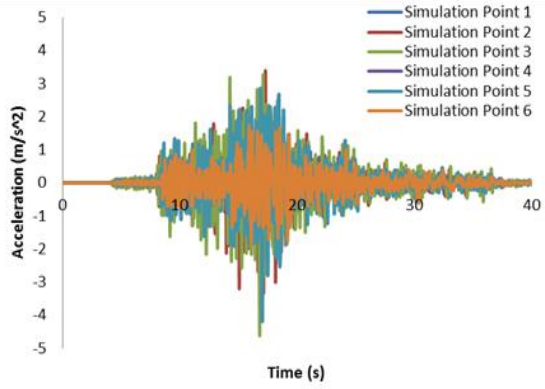


(b)

**Fig. 3.** (a) Acceleration response spectrum considering wave-passage, incoherency and local site effect, (b) Simulated time series

**Table 6**. Natural period and frequency of the structure for the first 4 modes

| | Period (second) | | Frequency (rad/sec) | |
|---|---|---|---|---|
| No. of modes | Current study | Tondini and Stojadinovic | Current study | Tondini and Stojadinovic |
| Mode 1 | 1.956 | 1.967 | 3.19 | 3.21 |
| Mode 2 | 1.948 | 1.953 | 3.20 | 3.22 |
| Mode 3 | 0.802 | 0.83 | 7.72 | 7.83 |

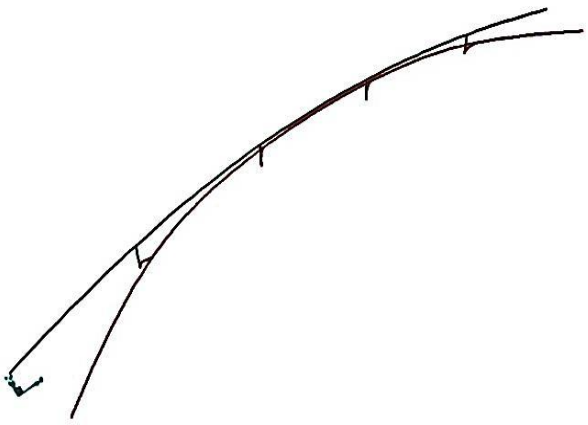

(a) The first mode shape

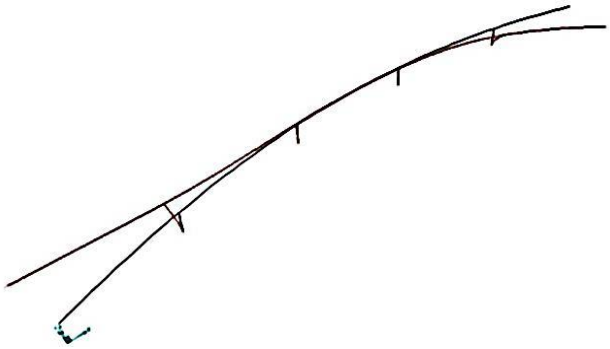

(b) The second mode shape

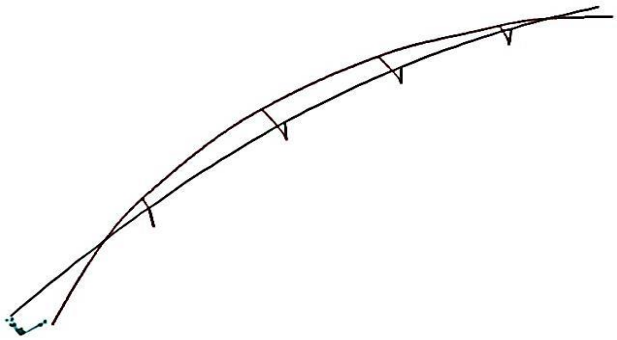

(c) The third mode shape

**Fig. 4.** The explanation of (a), (b), and (c) are separately presented

### *3.3 Analysis and Discussions*

To survey the directionality effect of the SVGMs on the dynamic response of the bridge, time history analysis was performed for various angles of incidence, and some significant responses were selected and discussed.

#### *3.3.1 Axial Force*

Figures 5 (a), (b), (c), and (d) show the variation of column's maximum axial force under uniform (U) and non-uniform (NU) excitations and for different incidence angles. It is evident that the responses of the bridge are different for uniform and non-uniform excitations, while for several cases, the responses due to SVGMs excitations are more than uniform. The maximum response occurred for column 3 under non-uniform excitation. Interestingly, the first column responses caused by uniform excitation are predominant in all input angles, while for columns 2, and 3 that are situated on the soft soils, the responses from SVGMs excitations are exceed the results from uniform excitations. Moreover, it is evident that for column 2, the maximum response was recorded at an input angle of 0.0 and for column 3 at 90 degrees, which is logical because of the symmetric and curved shape of the bridge plan. Regarding the wave propagation way from simulation point 1 to 6, the effects of SVGMs on the response of the bridge is noticeable. Also, it is not possible to indicate a critical incidence angle for all columns.

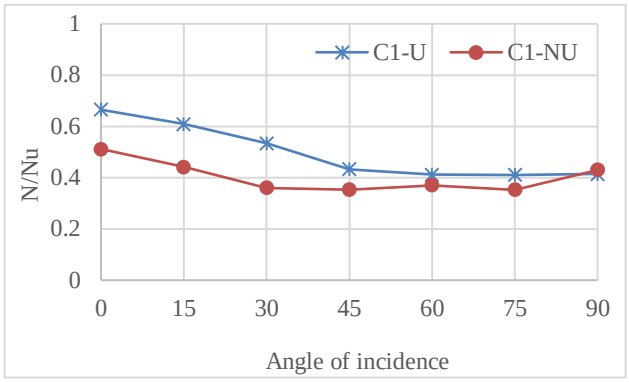


(a)

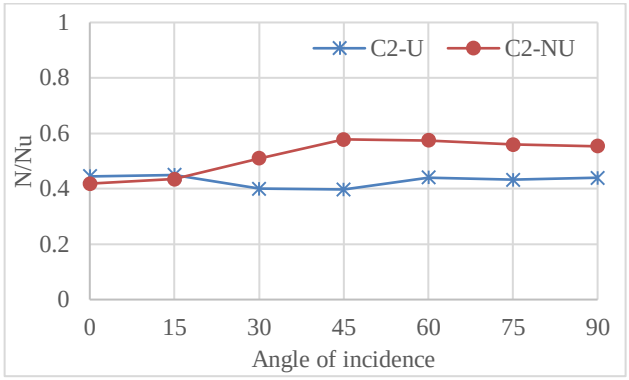


(b)

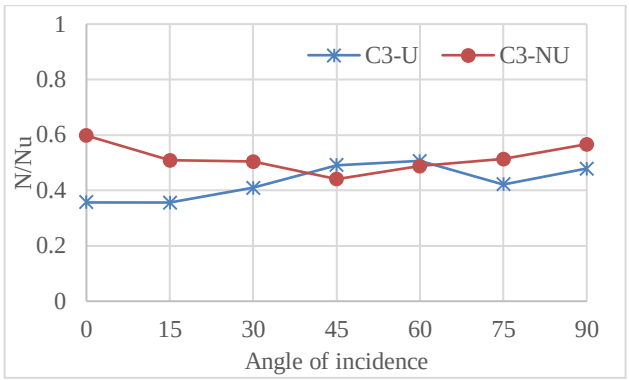


(c)

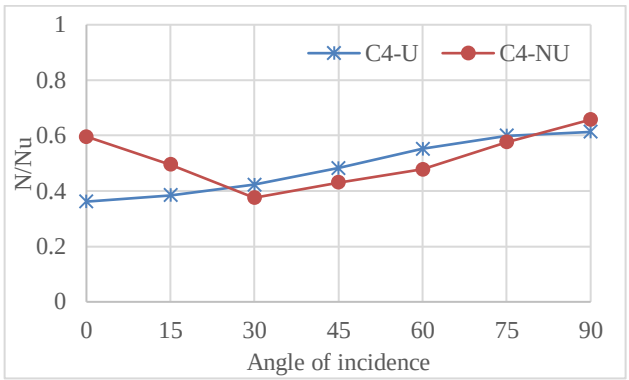


(d)

**Fig. 5** : Normalized Axial Force vs. Angle of incidence under uniform (U) and non-uniform (NU) excitations

*3.3.2 Moments*

Figures 6 (a) to (h) illustrate the maximum moment response of columns under uniform (U) and non-uniform (NU) excitations for various seismic angles of incidence in longitudinal and transverse directions. From the results, it is clear that the response of the bridge is affected by the angle of incidence. For the longitudinal direction, the moment responses caused by uniform excitation are exceed the responses caused by non-uniform excitations. But in the transverse direction, and column 4, the maximum moment response occurred due to non-uniform excitation. From the results, in the longitudinal direction, the maximum responses occurred at 60 degrees while the same results in the transverse order occurred at 30 degrees.

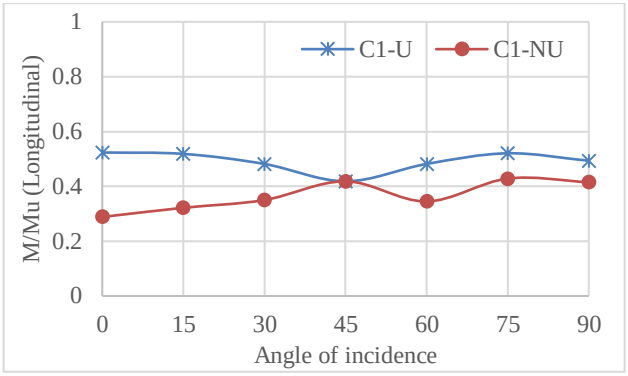


(a)

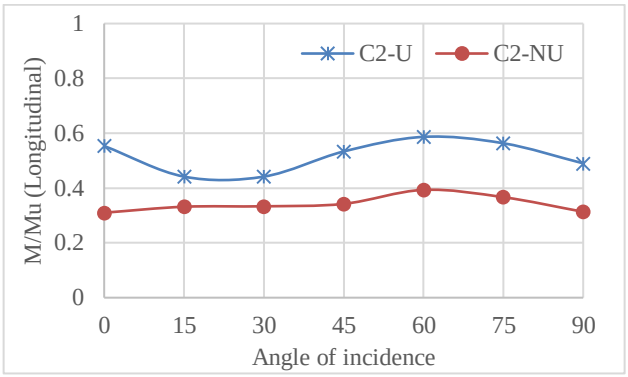


(b)

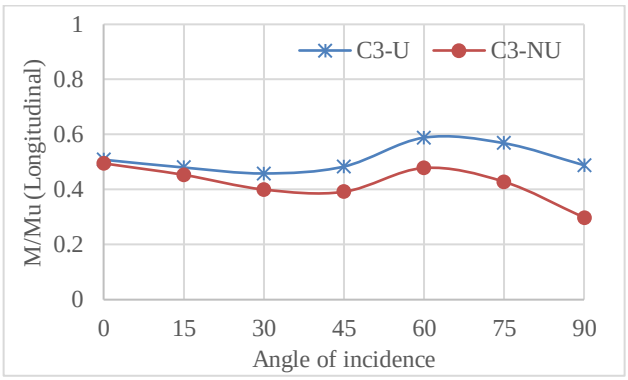


(c)



[ DOR: 20.1001.1.23454296.2022.6.3.3.8 ]
[ DOI: 10.52547/nmce.6.3.64 ]

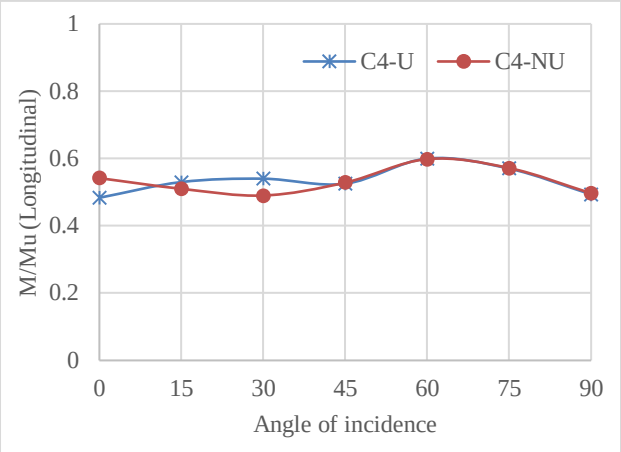


(d)

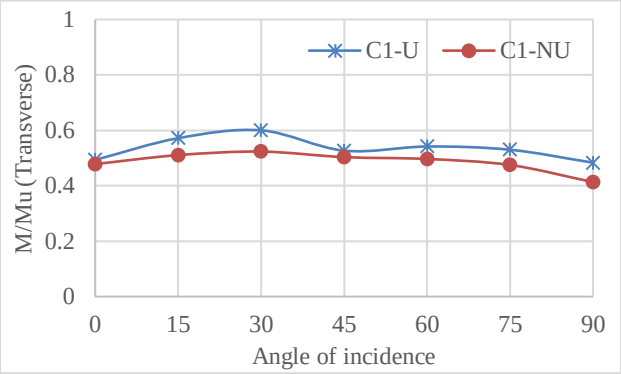


(e)

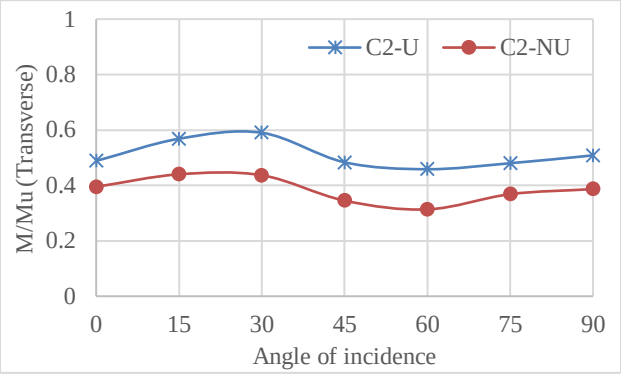


(f)

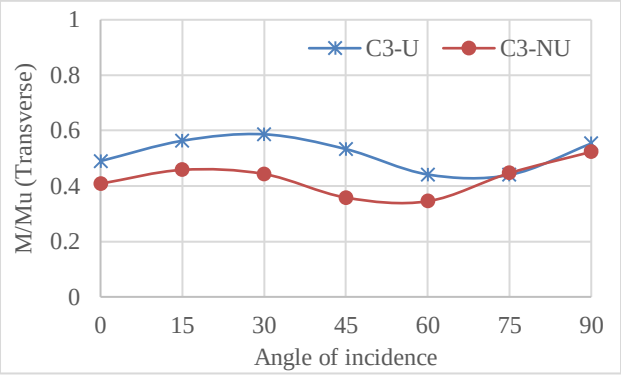


(g)

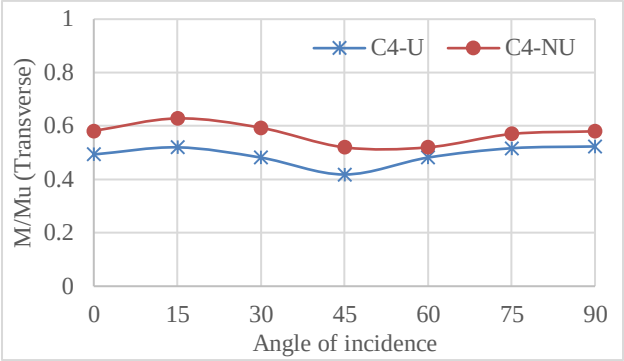


(h)

**Fig. 6** : Normalized Moment vs. Angle of incidence under uniform (U) and non-uniform (NU) excitations in longitudinal and transverse directions

*3.3.3 Drift*

Figures 7 (a) and (b) illustrate the variety of column drift ratios and drift response ratio under uniform (U) and non-uniform (N) excitations, respectively, for different angles in the transverse direction. The drift response ratio is defined as:

$$\frac{drift\ response\ ocuurred\ at\ the\ angle\ of\ incidence: \theta}{drift\ response\ ocuurred\ at\ the\ angle\ of\ incidence: 0}$$

The drift ratio of the columns is one of the most representative responses to explore the effects of SVGMs. From Figure 7(a), the total manner of drift responses corresponding to the variations of input angle are almost the same. It is interesting, that the maximum drift ratio occurred for column 4, and the corresponding angle is 15 degrees. However, in Figure 7(b), the maximum drift response ratio was recorded for column 3 due to non-uniform excitations. Regarding Figure 7 (b), it is evident that column 3 is more sensitive to the variation of the seismic angle of incidence in comparison with other columns. It is reasonable because the column was assumed to be situated on the soft soil, and the soil structure interaction increased the responses. But the acute member is column 4 and it is clear that the drift response increased due to SVGMs. The corresponding critical angles are 15 and 60 degrees.

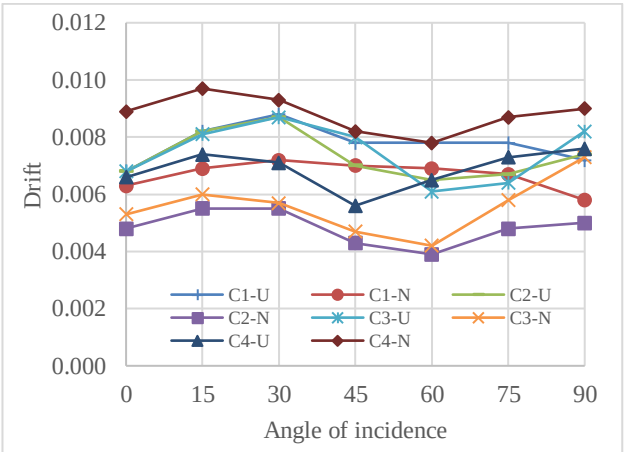


(a)

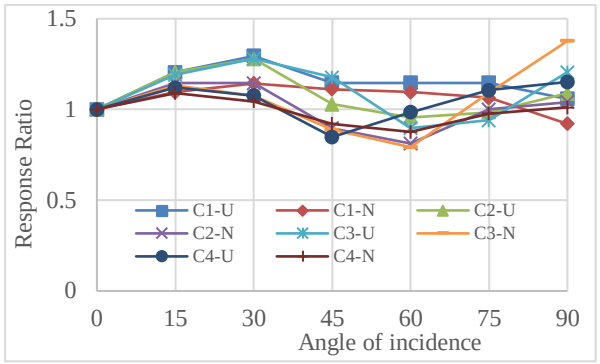


(b)

**Fig. 7.** (a): Drift ratio vs. Angle of incidence, (b): Drift response ratio vs. Angle of incidence

### *3.3.4 Base Shear*

Figures 8 (a) and (b) depict the variation of base shear for different angles of incidence under uniform and non-uniform excitations in longitudinal and transverse directions. The variations of base shear for uniform and non-uniform excitations almost show the same trend. For longitudinal direction angle of incidence of 15 degrees and the transverse direction of 60 degrees indicate the maximum responses. The peak response occurred under non-uniform excitations. Figures 8 (c), (d), (e), and (f) show the sensitivity of columns to variation of input angles. The response ratios are calculated as the ratio of the response of the columns under the various angles of incidence to the zero angles. From Figure 8 (c), it is clear that column 1 is excited more than the other columns due to non-uniform excitations.

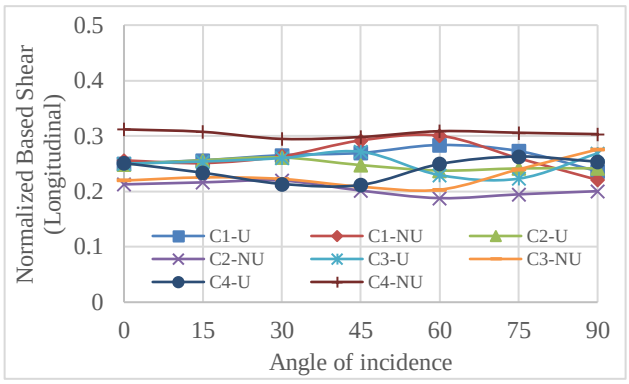


(a)

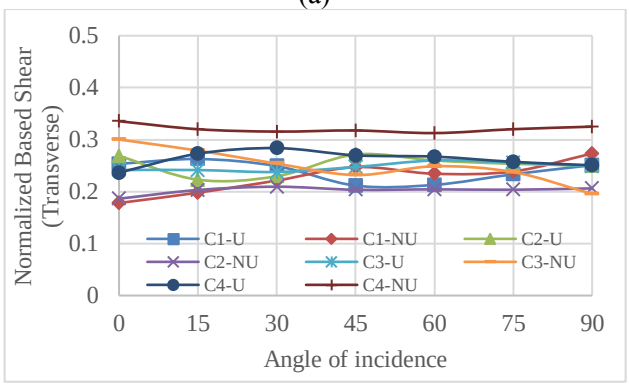


(b)

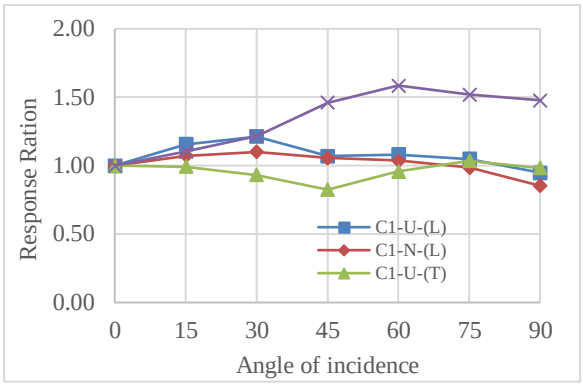


(c)

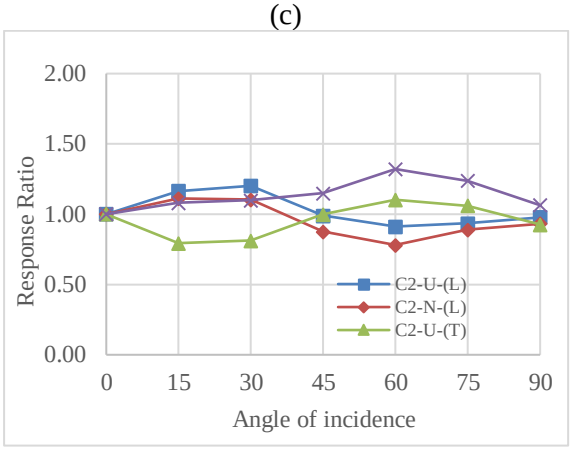


(d)

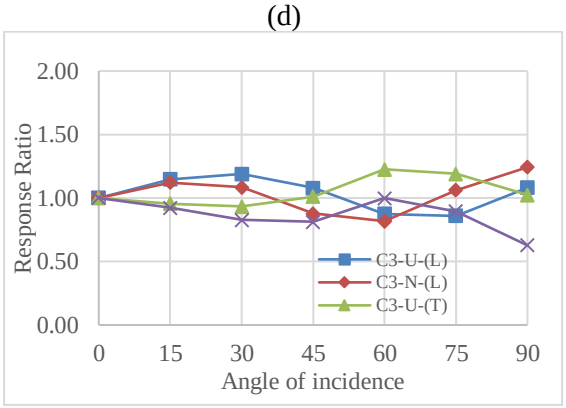


(e)

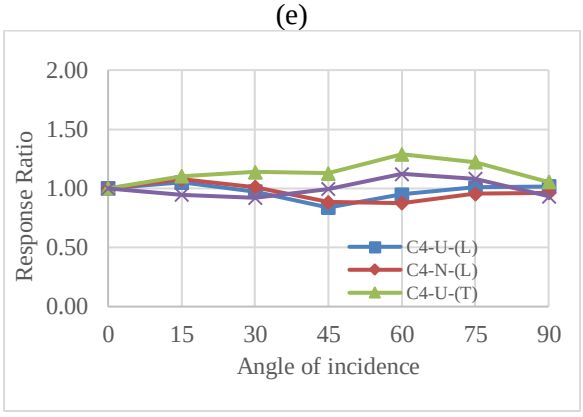


(f)

**Fig. 8** : (a) and (b): Base shear vs. Angle of incidence; (c), (d), (e) and (f) Base shear response ratio vs. Angle of incidence for Longitudinal (L) and Transverse (T) directions under uniform (U) and non-uniform (N) excitations.

### 3.3.5 IDA analysis

Some papers focused on the issue of the critical seismic angle of incidence, but almost all of them are limited to simple structures with a low degree of freedom. By increasing the degree of freedom especially for structures like the studied bridge, a simple applicable and straightforward method is necessary. So, in this section, an incremental dynamic analysis for various angles of incidence was performed to survey the non-linear behavior of the columns and to find the critical input angle under uniform and non-uniform excitations. The performance levels corresponding to damage states and drift limits are considered as presented in Table 7 [33,34,35]. The bridge was analyzed for original, and simulated records for different PGA levels and the relative drift ratios of the columns monitored. The drift ratio of less than 0.2% is considered as no damage state or immediate occupancy. The drift ratio of more than 0.2% and less than 0.5% is defined as repairable or damage control. The life-safe condition or damage state is considered for drift ratio of more than 0.5% and less than 1.5%. The drift ratio of more than 1.5% and less than 2.5% describes severe damage.

**Table 7.** Performance levels corresponding damage states and drift limits [34]

| Performance level | Damage state | Drift |
|---|---|---|
| Fully operational, Immediate occupancy | No damage | <0.2% |
| Operational, Damage control, Moderate | Repairable | <0.5% |
| Life safe-Damage state | Irreparable | <1.5% |
| Near collapse, Limited safety | Severe | <2.5% |
| Collapse | | >2.5% |

Figures 9 (a), to (h), illustrate the IDA curves of the bridge piers under uniform (U), and non-uniform (N), movements for different seismic angles of incidence. From Figures (a - f) it is clear that the predominant load pattern for columns 1, 2, and 3 is uniform excitation and life safety performance level occurred at PGA about (0.6-0.65)g. For column 4, the life safety performance level occurred under non-uniform excitation, and for PGA level, about 0.55g. Also, from the results, the life safety performance level for each column occurred at a different seismic incidence angle. For example, the critical seismic incidence angle for column 4, for uniform and non-uniform excitations is 60 and 15 degrees, respectively. The total trend represents that by increasing the distances from the first simulation point and subsequently enhancing the SVGMs effects decreased the required PGA level to a specific performance level. It means that the reliability of the bridge was reduced under non-uniform excitations.

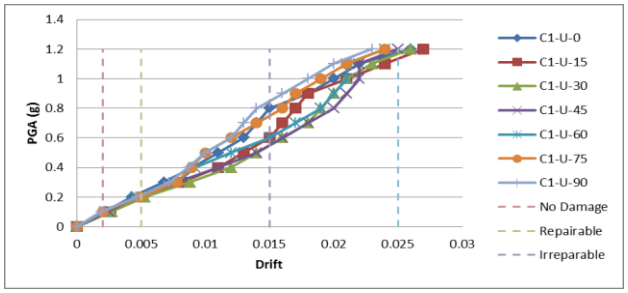


(a)

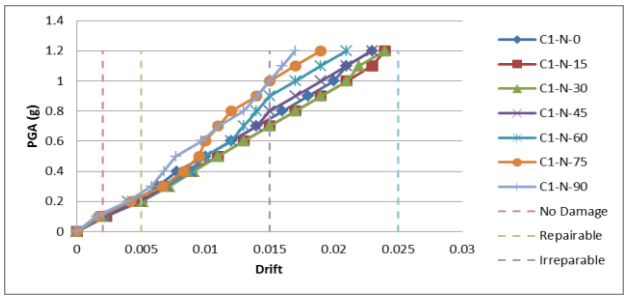


(b)

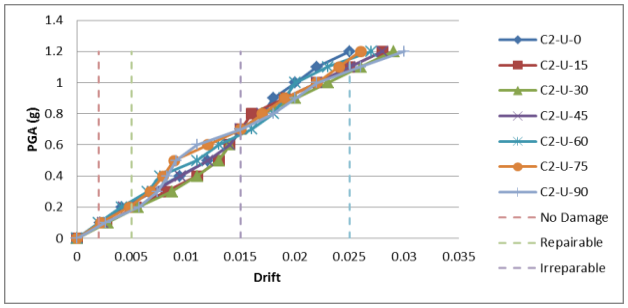


(c)

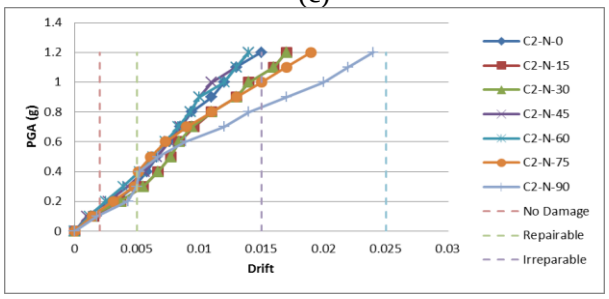


(d)

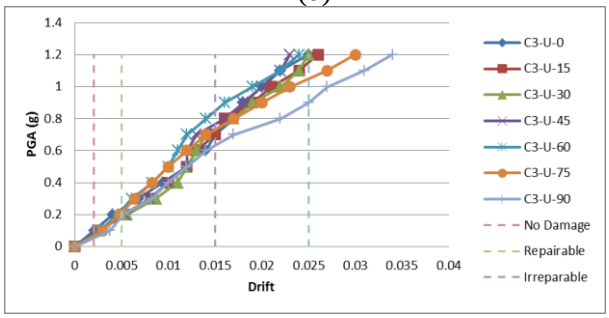


(e)


[ DOR: 20.1001.1.23454296.2022.6.3.3.8 ]
[ DOI: 10.52547/nmce.6.3.64 ]

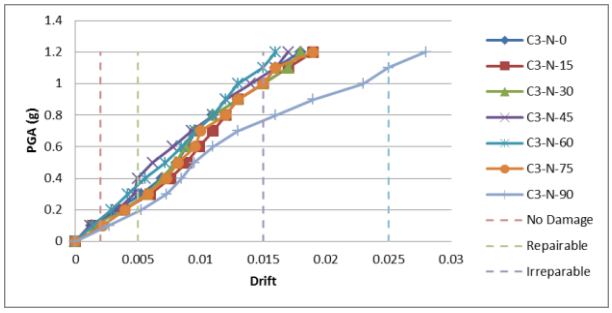


(f)

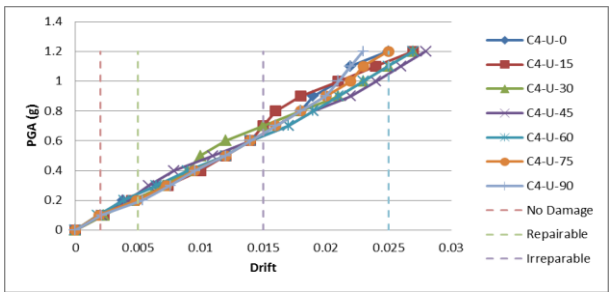


(g)

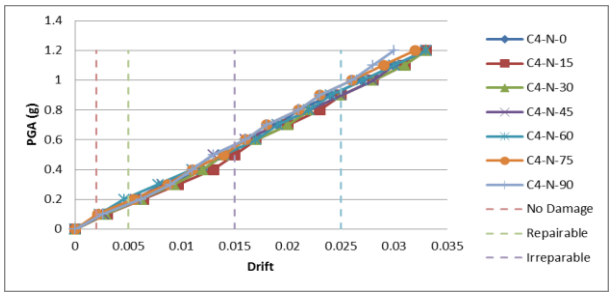


(h)

**Fig. 9** : (a) to (b): IDA curves for columns under uniform (U) and non-uniform (N) excitations in longitudinal (L) and transverse (T) directions for different angles of incidence

### *3.3.6 Fragility Curves*

In this section, based on the results of IDA analysis, the corresponding fragility curves are developed and illustrated in Figure 10. The graphs represent damage exceedance probability for different PGA levels. The life safety (L.S.) performance level is considered to evaluate the fragility of the studied bridge under spatially varying ground motions for various seismic incident angles. From the result, it is clear that the critical input angle is not the same for different columns. This result attributed to the irregular shape of the bridge deck. Regarding Figures 10 (a) to (h), recognizing that the critical seismic input angle is related to the PGA level, for a low PGA level, the maximum responses occurred in the longitude direction. By increasing the PGA level, the transverse direction responses increased remarkably.

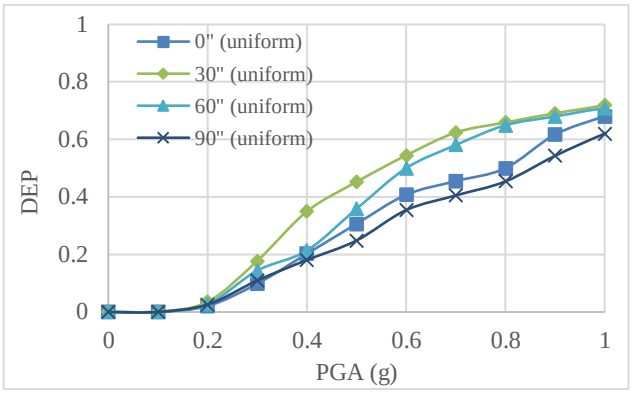


(a) Column 1 (Uniform-L.S.)

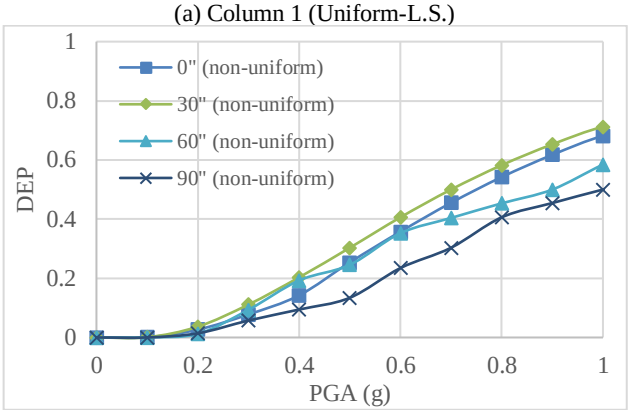


(b) Column 1 (Non-Uniform-L.S.)

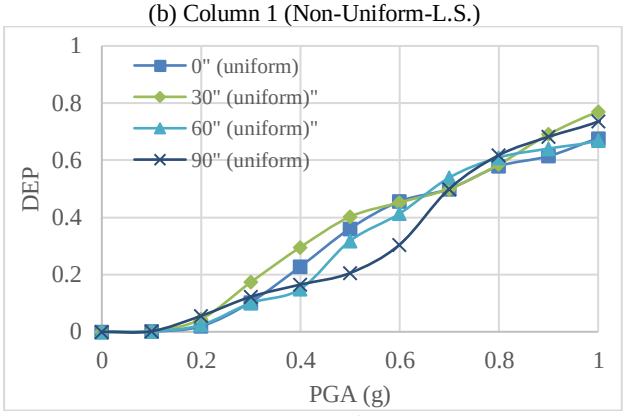


(c) Column 2 (Uniform-L.S.)

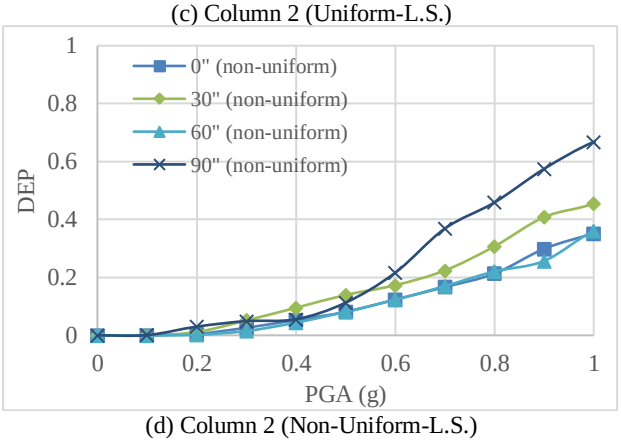


(d) Column 2 (Non-Uniform-L.S.)


[ DOR: 20.1001.1.23454296.2022.6.3.3.8 ]
[ DOI: 10.52547/nmce.6.3.64 ]

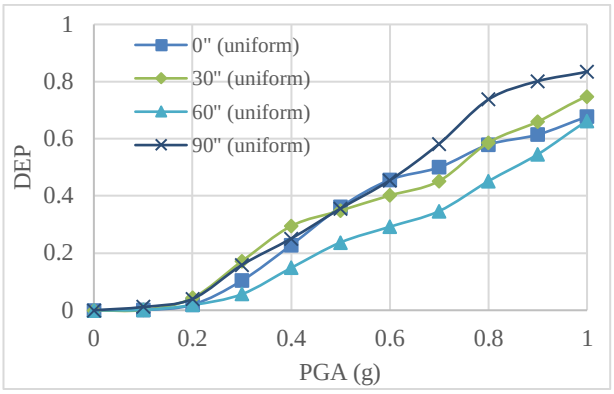

(e) Column 3 (Uniform-L.S.)

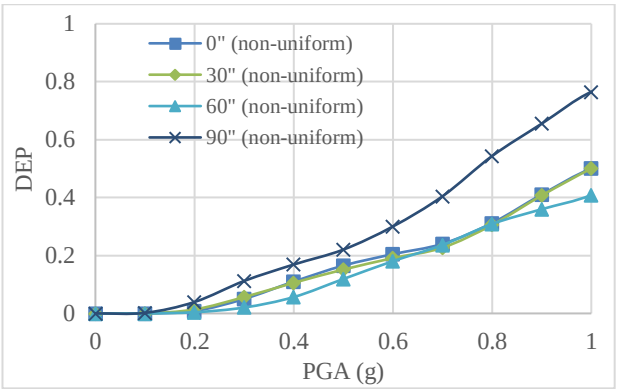

(f) Column 3 (Non-Uniform-L.S.)

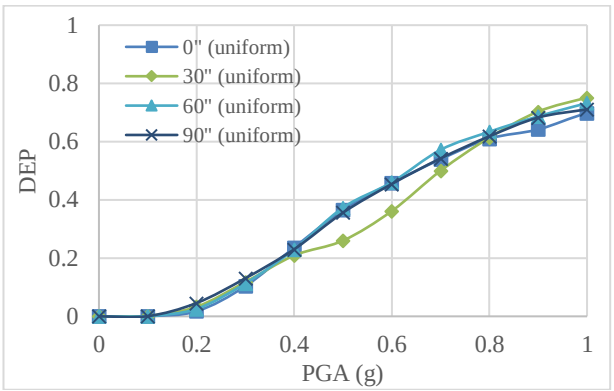

(g) Column 4 (Uniform-L.S)

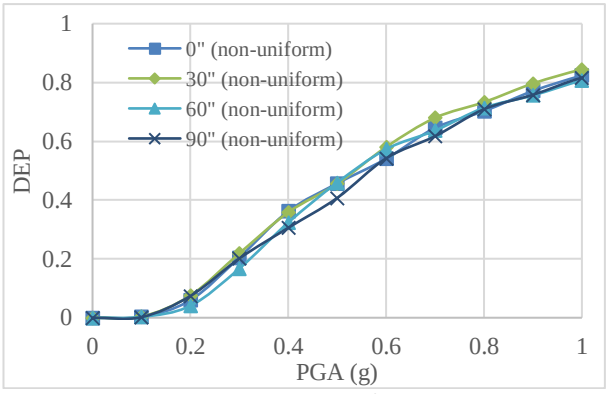

(h) Column 4 (Non-Uniform-L.S.)

**Fig. 10** : Fragility curves for uniform and non-uniform excitations under different seismic input angles. DEP: damage exceedance probability- L.S. : life safety

The damage exceedance probability for the first and second simulation point under uniform excitations is predominant, but results from the third and fourth simulation point indicate that by increasing the distance from the first simulation point, the effects of SVGMs components caused the damage exceedance probability under non-uniform excitations to be predominant. Based on the results, the critical incident angle under uniform and non-uniform excitations for columns 1 and 4 occur at 30 degrees, while the same results for columns 2 and 3 are different. The critical seismic input angle for two middle columns occurs at 90 degrees under non-uniform excitations. The vital point extracted from Figures 10 (d) and (f) where the damage exceedance probability under non-uniform excitations increased remarkably compared to the same results from uniform excitations. It means that for columns situated on soft soils, the SVGMs components enormously enhance the responses. Totally, from the results, the maximum responses for the studied bridge were recorded at 30 degrees in longitude and 90 degrees in transverse directions.

## 4. Conclusion

In this paper, a non-uniform and uniform time history analysis of a curved bridge under various seismic incidence angles was performed. A simulation technique mentioned in section 2, implemented to simulate the required time series and 20 series of generating arrays, were imposed on the structure. It is challenging to introduce a significant and minor seismic incidence angle because the responses are very different. Moreover, based on the results, it is interesting that in the case of non-uniform excitation and different soil condition, the responses increased noticeably because of soft soils.

a) From the results, it is clear that the response of the structure was affected by varying the seismic angle of incidence, and in some cases the responses increased significantly.

b) In this study, the soil condition is assumed different at the simulation points. Based on the outcomes, the soft soil conditions remarkably amplify the bridge responses.

c) In addition, based on the outcomes, the maximum response for each pier of the bridge occurs at an independent seismic input angle under uniform and non-uniform excitations.

d) Moreover, the results revealed that the critical input angle for non-uniform and uniform excitation is different. In several cases under non-uniform movements, the responses recorded were remarkably more than the results from uniform excitations.

e) IDA analysis result revealed that by getting far from the first simulation point and subsequently enhancing the SVGMs parameters, the responses under non-uniform

excitations become predominant, and the orientation of critical input angle changes from longitude to transverse.

f) The results show that the critical input angle in longitude direction under uniform and non-uniform excitations are about 30 degrees while in transverse direction the input angle of 90 degrees caused the maximum responses under-nonuniform excitations.

## References

**[1]** Tseng, W.S. and Penzien, J. (1975), "Seismic response of long multiplespan highway bridges", Earthquake Engineering and Structural Dynamics, 4 (1), 25-48.

**[2]** Williams, D. and Godden, W. (1979), "Seismic response of long curved bridge structures: experimental model studies", Earthquake Engineering and Structural Dynamics, 7 (2), 107-128.

**[3]** Kawashimak, K., Penzien, J. (1979), "Theoretical and experimental dynamic behavior of a curved model bridge structure", Earthquake Engineering and Structural Dynamics, 7 (2), 129-145.

**[4]** Li, G.H., Shi, D. and Heins, C.P. (1984), "The finite element method of the seismic analysis of the curved bridge", Journal of Tongji University: Natural Science, 23 (1), 1-21.

**[5]** Yuan, W.C., Wang, Y.G., Yang, Y.M. (1996), "Spatial seismic response analysis on the curved girder bridges", In: Proceedings of the 12th National Bridge Academic Conference, Shanghai, 1996.

**[6]** Zhu, D.S., Liu, S.Z. and Yu, L.S. (2002), "Research on seismic response of curved girder bridges", China Journal of Highway and Transport, 15 (3), 42-48.

**[7]** Fan, L.C., Nie, L.Y. and Li, J.Z. (2003), "Discussion on standard of critical angle of seismic wave in seismic analysis of complicated structures", Journal of Tongji University: Natural Science, 31 (6), 631-636.

**[8]** Saad, A.S., Sanders, D.H. and Buckle, L.G. (2012), "Effect of rocking foundations on seismic behavior of horizontally curved bridges with different degree of curvatures", In: Proceedings of 15th World Conference on Earthquake Engineering, Lisbon, September.

**[9]** Torbol Marco and Shinozuka Masanobu. (2012), "Effect of the angle of seismic incidence on the fragility curves of bridges" Earthquake Engineering and Structural Dynamics, 41, 14, 2111-2124.

**[10]** Wang, Yuandong., Ibarra, Luis. And Pantelides, Chris. (2017), "Effects of Ground Motion Incidence Angle in Reinforced Concrete Skewed Bridge Retrofitted with Buckling Restrained Braces" Department of Civil and Environmental Engineering, The University of Utah.

**[11]** Aparma Roy, Gautam Bhattachrya and Rana Roy, (2017) "Maximum credible damage of RC bridge pier under bi-directional seismic excitation for all incidence angles" Engineering Structures, 152, 251–273. 10.1016/j.engstruct.2017.09.008

**[12]** Soleimani Farahnaz, Brani Vidakovic, Reginald DesRoches and Jamie Padgett. (2017) "Identification of the significant uncertain parameters in the seismic response of irregular bridges" Engineering Structures, 141, 356–372, 10.1016/j.engstruct.2017.03.017

**[13]** H.R. Noori, M.M. Memarpour, M. akhchalian and S. Soltanieh. (2019) "Effects of ground motion directionality on seismic behavior of skewed bridges considering SSI" Soil Dynamics and Earthquake Engineering, 127, 105820, 10.1016/j.soildyn.2019.105820

**[14]** S. Soltanieh, M.M. Memarpour and F. Kilanehei. (2019) "Performance assessment of bridge-soil-foundation system with irregular configuration considering ground motion directionality effects" Soil Dynamics and Earthquake Engineering, 118, 19–34. 10.1016/j.soildyn.2018.11.006

**[15]** Yuandong Wang, Luis Ibarra and Chris Pantelides. (2020) "Effect of incidence angle on the seismic performance of skewed bridges retrofitted with buckling-restrained braces" Engineering Structures, 211, 110411. 10.1016/j.engstruct.2020.110411

**[16]** Ruiwei Feng, Tongfa Deng, Tianpeng Lao, Anastasios G. Sextos, Wancheng Yuan. (2020) "Theory and experimental verification of a resultant response-based method for assessing the critical seismic excitation direction of curved bridges" Engineering Structures, 216, 110713. 10.1016/j.engstruct.2020.110713

**[17]** María Elisa Ramos-Sepúlveda and Ashly Cabas. (2021) "Site Effects on Ground Motion Directionality: Lessons from Case Studies in Japan" S.D.E.E., 147, 106755. 10.1016/j.soildyn.2021.106755

**[18]** Saxena V. Deodatis G. and Shinozuka M. (2000), "Effect of spatial variation of earthquake ground motion on the nonlinear dynamic response of highway bridges" Proc of 12th World Conf on Earthquake Engineering, Auckland, New Zealand, January.

**[19]** Vanmarcke EH. and Fenton GA. ( 1991), "Conditioned simulation of local fields of earthquake ground motion", Structural Safety, 10, 247–264.

**[20]** Kameda H and Morikawa H. (1992), "An interpolating stochastic process for simulation of conditional random fields", Probabilistic Engineering Mechanics, 7, 243–254.

**[21]** Liao S. and Zerva A. (2006)," Physically compliant, conditionally simulated spatially vriable seismic ground motions for performance-based design", Earthquake Engineering and Structural Dynamics, 35, 891–919.

**[22]** Konakli K. and Der Kiureghian A, (2012), "Simulation of spatially varying ground motions including incoherence, wave-passage and site-response effects" Earthquake Engineering and Structural Dynamics, 41: 495-513. doi.org/10.1002/eqe.1141

**[23]** Luco JE. and Wong HL. (1986), "Response of a rigid foundation to a spatially random ground motion" Earthquake Engineering and Structural Dynamics, 14, 891–908.

**[24]** Der Kiureghian A and Neuenhofer A. (1992), "Response spectrum method for multiple support seismic excitation", Earthquake Engineering and Structural Dynamics, 21, 713–740.

**[25]** Zerva A. and Harada T. ( 1994),"A site specific model for the spatial incoherence of the seismic ground motions",



[ DOR: 20.1001.1.23454296.2022.6.3.3.8 ]
[ DOI: 10.52547/nmce.6.3.64 ]

Proceedings of the 5th National Conference on Earthquake Engineering, Chicago, Illinois, July.

**[26]** Ketchum M, Chang V, and Shantz T. (2004), "Influence of design ground motion level on highway bridge costs" Pacific Earthquake Engineering Research Center, Berkeley, CA, USA.

**[27]** McKenna F and Fenves GL. (2000), "An object-oriented software design for parallel structural analysis", *In: Proceedings of the advanced technology in structural engineering*, Structures Congress, ASCE,Washington,DC.

**[28]** Tondini N and Stojadinovic B. (2012), "Probabilistic seismic demand model for curved reinforced concrete bdidges" Bull Earthquake Eng. 10, 1455-1479.

**[29]** Amjadian M. and Agrawal A. K. (2017), "Dynamic characteristics of horizontally curved bridges" *Journal of Vibration and Control*, 1–19.

**[30]** Zhang J and Makris N. (2002a), "Kinematic response functions and dynamic stiffness of bridge embankments", *Earthquake Engineering and Structural Dynamics*, 31, 1933–1966.

**[31]** Zhang J, Makris N and Delis E. (2004), "Structural characterization of modern highway overcrossings—a case study", *Journal of Structural Engineering, ASCE* , 130(6), 846–860.

**[32]** Toki K. and Yanabu K. (1988), "Detection of apparent wave velocity in near surface ground with irregular profile by an array observation", *Proceeding of 9th World Conf on Eearthquake Eengineering*, Tokyo.

**[33]** Ghobarah, Ahmed. (2001) "Performance-based design in earthquake engineering: state of development" Engineering Structures 23, 878–884.

**[34]** Arash E. Zaghi, Siavash Soroushian, E. "Manos" Maragakis, Alicia Echevarria, Yuan Tian, and Andre Filiatrault. Seismic Fragility Study of Fire Sprinkler Piping Systems with Grooved Fit Joints. J. Struct. Eng., 2015, 141(6): 04014157.

**[35]** Arash E. Zaghi, Joseph Wieser, Manos Maragakis, and Ian Buckle. A Methodology for the Experimental Evaluation of Seismic Pounding at Seat-Type Abutments of Horizontally Curved Bridges. Structures Congress 2012 © ASCE 2012.





[ DOR: 20.1001.1.23454296.2022.6.3.3.8 ]

[ DOI: 10.52547/nmce.6.3.64 ]